HHS Public Access

Author manuscript

J Immunol. Author manuscript; available in PMC 2017 February 02.

Published in final edited form as:

J Immunol. 2016 February 01; 196(3): 1293–1304. doi:10.4049/jimmunol.1500931.

Dietary Vitamin D_3 suppresses pulmonary immunopathology associated with late stage tuberculosis in C3HeB/FeJ mice

Allison E. Reeme[*] and **Richard T. Robinson**[*,†]

[*]Department of Microbiology and Molecular Genetics, Medical College of Wisconsin, Milwaukee, Wisconsin 53226, USA

Abstract

Tuberculosis (TB) is a significant human disease caused by inhalation of *Mycobacterium tuberculosis* (Mtb). Left untreated, TB mortality is associated with a failure to resolve pulmonary immunopathology. There is currently widespread interest in using Vitamin D_3 ($VitD_3$) as an adjunct therapy for TB, as numerous *in vitro* studies have shown that $VitD_3$ has direct and indirect mycobactericidal activities. However, to date there have been no *in vivo* studies addressing whether $VitD_3$ affects experimental TB outcome. Here we use C3HeB/FeJ mice to determine if dietary $VitD_3$ influences the outcome of experimental TB. We observed that although Mtb burdens did not differ between mice on a $VitD_3$-replete diet ($VitD^{HI}$ mice) and mice on a $VitD_3$-deficient diet ($VitD^{LO}$ mice), the inflammatory response in $VitD^{HI}$ mice was significantly attenuated relative to $VitD^{LO}$ controls. Specifically, the expression of multiple inflammatory pathways was reduced in the lungs at later disease stages, as were splenocyte IL12/23p40- and IFNγ-levels following *ex vivo* restimulation. Dietary $VitD_3$ also suppressed the accumulation of T cells in the mediastinal lymph nodes and lung granulomatous regions, while concomitantly accelerating the accumulation of $F4/80^+$ and $Ly6C/Ly6G^+$ lineages. The altered inflammatory profile of $VitD^{HI}$ mice also associated with reductions in pulmonary immunopathology. VitD receptor deficient ($vdr^{-/-}$) radiation bone marrow chimeras demonstrate that reductions in pulmonary TB-immunopathology are dependent on hematopoietic VitD-responsiveness. Collectively, our data support a model wherein the *in vivo* role of $VitD_3$ during TB is not to promote Mtb killing, but rather to function through hematopoietic cells to reduce Mtb-elicited immunopathology.

INTRODUCTION

Tuberculosis (TB) is a significant human disease caused by aerogenic transmission of the intracellular pathogen *Mycobacterium tuberculosis* (Mtb), which primarily infects phagocytes in the lung alveoli (1). Recent data from the World Health Organization (WHO) demonstrate there were ~9.6 million new TB cases in 2014, with 1.5 million individuals dying from TB in the same year (2). Improved socioeconomic conditions, public health practices and use of standard short-course chemotherapy have reduced the global TB death rate by 45% since 1990, and have helped the WHO achieve its goal of reversing TB incidence by 2015 (2). However, the treatment options available for TB and increasingly

[†]Corresponding author: rrobinson@mcw.edu; Phone: 414-955-2976; Fax: 414-955-6535.

common multidrug-resistant TB (MDR TB) remain limited and are often complicated by poor patient compliance due to long treatment durations (2). For these reasons, new or adjunctive therapies that shorten treatment or improve treatment outcome are greatly needed and required for the WHO to reach its goal of eliminating TB by 2050 (3).

Host resistance to TB is promoted by a T_H1 response that is initiated by lung resident phagocytes following their internalization of Mtb bacilli; after these phagocytes migrate and present Mtb antigen (Ag) in the draining mediastinal lymph nodes (MLNs), Ag-specific T cells accumulate and the lungs develop granulomas comprising both mononuclear and polymorphonuclear lineages (1). In experimental TB there is a delay in Ag-specific T cell activation (4), allowing for dissemination of Mtb to extrapulmonary sites. Phagocyte production of IL12 is essential for activation of T cells and their subsequent production of IFNγ and TNFα (5, 6), which are the two major T_H1 cytokines that promote macrophage killing of intracellular Mtb (1). The necessity of IFNγ during infection is highlighted by the observation that T cells incapable of IFNγ-production are unable to control Mtb burdens (5, 7). Paradoxically, although T_H1 responses are required to control Mtb, pulmonary inflammation comes at the expense of immunopathology that is potentially fatal to the host (8, 9). In animal models, this is evidenced by the post-infection mortality of mice deficient in IL27R (10) or PD1 (11, 12), both of which function to suppress T_H1 responses. In humans, the danger of immunopathology is evidenced by the morbidity and mortality associated with a failure to resolve lung immunopathology (13). Given the negative consequences of too little or too much inflammation, adjunctive TB therapies must create and/or support an immune environment that can effectively contain the bacteria without damaging the lung or other organs. While adjunct immunosuppressive therapies can enhance antibiotic efficacy (14), others can reduce immunopathology and markedly improve animals' survival even in the absence of effecting Mtb burden (15).

There is currently widespread interest in using Vitamin D_3 ($VitD_3$) as an adjunctive therapy for TB (16). $VitD_3$ is a fat-soluble secosteroid that can be obtained through the diet or synthesized in the skin. $VitD_3$ enters the circulation and is hydroxylated in the liver to form 25-OH hydroxyvitamin D_3 (25(OH)D) (17). 25(OH)D can either freely diffuse into target cells or bind the VitD binding protein (VDBP) and enter cells via receptor-mediated endocytosis (18). 25(OH)D must then undergo a second hydroxylation by 25-hydroxyvitamin D 1α hydroxylase (CYP27b1) to form $1,25(OH)_2$ dihydroxyvitamin D ($1,25(OH)_2D$), the biologically active form referred to as VitD. VitD binds the vitamin D receptor (VDR) in the cytosol and translocates into the nucleus where it binds VitD response elements (VDREs) on the DNA and regulates transcription of multiple genes in both hematopoietic and non-hematopoietic cell types (17). After it was discovered that both sun-exposure and animal fat consumption (e.g. butter, cod liver oil) are sources of $VitD_3$, it was widely reasoned that $VitD_3$ contributed to the therapeutic efficacy of these early TB treatments (19). VitD's direct bactericidal effect on Mtb has been studied *in vitro* (20, 21), as have VitD's indirect bactericidal effects on Mtb-infected human monocyte/macrophage (MØ) cultures (22–24). These *in vitro* studies have led to the following prevailing model (25): Following TLR2/1 recognition of Mtb, MØs increase their expression of VDR and CYP27B1 (22); any 25(OH)D that enters the MØ is then converted to VitD, binds the VDR, translocates to the nucleus and through synergy with IFNγ increases production of

cathelicidin - an antimicrobial peptide that is directly cytotoxic to Mtb (26). However, despite the number of *in vitro* studies that point to $VitD_3$ and its metabolites as having both direct and indirect bactericidal activities, several large clinical trials have demonstrated that $VitD_3$'s effect on sputum conversion is largely nil (27–30). These negative data raise the question of what if any role does $VitD_3$ have during TB *in vivo*.

The goal of this study was to determine what effect dietary $VitD_3$ has on the outcome of experimental TB. This determination is important given the current interest in using $VitD_3$ as an adjunct therapy for TB, despite its effect on TB never having been tested in an *in vivo* model. Specifically, we used the C3HeB/FeJ model of TB to compare several key experimental TB readouts in the presence or absence of dietary $VitD_3$. Among mouse models of TB, the C3HeB/FeJ strain is considered by many to be the best at recapitulating the pathology observed in human TB (31–35). Given the number of *in vitro* studies demonstrating that VitD has both direct and indirect bactericidal effects, we began our study with the hypothesis that dietary $VitD_3$ would protect the host by reducing Mtb burden; we were surprised to observe this is not the case, and that instead $VitD_3$ protects the host by limiting TB-associated immunopathology. Collectively, our results demonstrate that dietary $VitD_3$ functions through hematopoietic lineages to suppress the pulmonary immunopathology associated with late stage TB.

MATERIALS AND METHODS

Mice

C3HeB/FeJ and B6.129S4-*Vdr*^{tm1Mbd}/J (i.e. *vdr*$^{+/-}$, (36)) breeder pairs were purchased from the Jackson Laboratory (Bar Harbor, ME) and bred at the Medical College of Wisconsin (MCW). All mice were treated according to National Institutes of Health and MCW Institute Animal Care and Use Committee (IACUC) guidelines.

Radiation bone marrow chimeras

vdr$^{+/+}$ and *vdr*$^{-/-}$ progeny were used to generate radiation bone marrow chimeras per our reported protocols, the percent reconstitution being ≥94% (5, 6). Mice were allowed 10 weeks to reconstitute prior to their use.

Experimental Diets

Beginning one month prior to infection, C3HeB/FeJ mice were fed specially formulated diets from Harlan Laboratories (Madison, WI) that contained either 0 IU $VitD_3$/gram ($VitD^{LO}$, #TD.89123), 2 IU $VitD_3$/gram ($VitD^{Std}$, #TD.1108) or 20 IU $VitD_3$/gram ($VitD^{HI}$, #TD.110799). These diets were chosen since their formulations were identical with the exception of $VitD_3$ and were similar to the diets used in other studies of dietary $VitD_3$ (37–39). For experiments involving *vdr*$^{-/-}$ and *vdr*$^{+/+}$ mice and radiation bone marrow chimeras: beginning at weaning and continuing throughout each experiment, *vdr*$^{-/-}$ and *vdr*$^{+/+}$ progeny were kept on a $VitD^{HI}$ "rescue diet" containing 20 $VitD_3$/gram and excess lactose (20% lactose; Harlan # TD.140326). Excess lactose is necessary to prevent the bone and immune abnormalities that would otherwise develop in *vdr*$^{-/-}$ mice (40–42).

Aerosol Infection

Mice were aerosol infected with virulent Mtb H37Rv per our reported protocols (5, 6). For bacterial load determinations, lungs and ½ spleen were removed and individually homogenized in normal sterile saline; serial dilutions of each homogenate were then plated on 7H11 and colonies counted after ≥ 2 weeks incubation at 37°C and 5% CO_2. Lungs from control mice were plated on day 1 post-infection to confirm the delivery of 46–108 bacteria per lung.

In vitro restimulation assay

Per the methods of Chackerian et al (43), ½ of each spleen from Mtb-infected $VitD^{HI}$ and $VitD^{LO}$ mice were collected at the indicated time points, pushed through a 70μm nylon screen and treated with sterile RBC lysis buffer. 2×10^6 cells per spleen in 2mL of complete RPMI media (RPMI + 10% FBS) were then stimulated with 1μg/mL concanavalin A (ConA) and live Mtb (H37Rv) at MOI=0, 0.5 or 1 for 48 hours. Supernatants were then collected, filtered through a 0.22μm filter and stored at −80°C until being assayed for murine IFNγ and IL12/23p40 by sandwich ELISA (BD Biosciences).

Histology and Morphometric Analysis

Lungs from Mtb-infected mice were formalin-fixed, paraffin-embedded and used for H&E and Acid Fast staining (Children's Hospital of Wisconsin Histology Core). Images were taken with a Labophot-2 upright microscope (Nikon, Tokyo, Japan) using a Retiga 2000R camera (QImaging; Surrey, BC, Canada); NIS Elements software (Nikon) was used for morphometric analysis (Supplemental Figure 1).

Immunohistochemistry

Paraffin embedded lungs were sectioned, deparaffinized, hydrated in deionized water, and treated with Target Retrieval Solution (DAKO, Carpinteria, CA) at either pH 9 (anti-CD3, anti-Foxp3, anti-Ly6C/Ly6G) or pH 6 (anti-F4/80). All slides were then stained using a DAKO Autostainer Plus (DAKO, Carpinteria, CA) with the standard labeled streptavidin-biotin protocol. Lung sections were stained at room temperature for 60 min with polyclonal rabbit anti-CD3 (DAKO; 1:100), anti-F4/80 (AbD Serotec; clone A3-1; 1:250), anti-Foxp3 (eBioscience, clone FJK-16s; 1:25) or anti-Ly6C/Ly6G (clone NIMP-R14; 1:250). Negative controls were performed with omission of the primary antibody. Slides were then developed with Tertiary Streptavidin-HRP (DAKO) and counterstained with hematoxylin.

Digital Immunochemistry Analysis

Immunohistochemistry stained slides were scanned on a high resolution, whole slide scanner (NanoZoomer HT 2.0, Hamamatsu, Japan) at 40× magnification. For image data quantification, images were imported into Visiopharm software (Visiopharm, Hørsholm, Denmark) and 20× region-of-interest (ROI) images were extracted to estimate detectable-antibody (DAB) positive areas. DAB negative areas were also measured to include in the total tissue area calculations. We utilized 4 ROIs per tissue section and morphometric analysis was performed. All images were processed with these preset thresholds and linear

Bayesian classification to generate a processed image (Supplemental Figure 2). Total DAB positive area per ROI (and total tissue area of the ROI) was measured in microns.

Flow cytometry

Mediastinal lymph node cells were prepared and stained for surface and intracellular markers per our previous protocols (5), using antibodies specific for CD4 (clone L3T4), CD8 (clone 53-6.7), IFNγ (clone XMG1.2) and TNFα (clone MP6-XT22) (BD Biosciences).

Quantitative Real Time PCR

Lung RNA was isolated from snap frozen tissue using the IBI Total RNA extraction kit (IBI Scientific, Peosta, IA). RNA was reverse transcribed using Applied Biosciences reagents (Life Technologies, Grand Island, NY) and the resulting cDNA was amplified using Bullseye Evagreen Master Mix (MidSci) and BioRad iQ5 detection system. The primer sequences used for cDNA amplification of *ifng*, *cyp27b1*, *cramp*, *vdr* and *gapdh* are listed in Supplemental Table 1. C_T values were determined using the BioRad iQ5 bundled software and all samples were normalized to *gapdh*. cDNA from specific time points was additionally used in the RT^2 Profiler PCR Array for Mouse Innate and Adaptive Immune Responses (Qiagen, Valencia, CA). Data was analyzed using the online RT^2 Profiler PCR Array data analysis software (Qiagen). All samples were normalized to at least one housekeeping gene between plates.

Statistics

For group analysis, two-way ANOVA with Bonferroni correction was used with $p<0.05$ considered significant. For all other experiments, unpaired Student's t-test was used to determine significance ($p<0.05$). All results are expressed as mean ± SD.

RESULTS

Dietary $VitD_3$ does not significantly affect bacterial burden during experimental TB

$VitD_3$ and $VitD_3$-metabolites are capable of killing Mtb *in vitro* via both direct and indirect mechanisms (20, 21, 25). To determine if dietary $VitD_3$ affects Mtb burden *in vivo*, adult C3HeB/FeJ mice were placed on either a $VitD_3$-replete ($VitD^{HI}$ mice) or $VitD_3$-deficient ($VitD^{LO}$ mice) diet for 30 days, aerosol-infected with 46–108 CFU of virulent Mtb (H37Rv), and kept on their respective diets for up to 110 days post-infection (Fig 1A). We then measured and compared organ CFU burden in $VitD^{LO}$ and $VitD^{HI}$ mice over a broad period of time post-infection. Standard CFU changes in C3HeB/FeJ mice were established by comparing $VitD^{LO}$ and $VitD^{HI}$ values to those of C3Heb/FeJ mice kept on standard mouse chow ($VitD^{Std}$ mice, Fig 1B–D). Throughout the entire time-course, plasma 25(OH)D levels were significantly higher in $VitD^{HI}$ mice relative to $VitD^{LO}$ and $VitD^{Std}$ mice; no differences in circulating Ca^{2+} and PO_4^{3-} levels were observed between $VitD^{LO}$, $VitD^{Std}$ and $VitD^{HI}$ mice (data not shown).

We observed that in both $VitD^{HI}$ and $VitD^{LO}$ groups, lung Mtb burdens increased logarithmically during the first 25 days post-infection (Fig 1B). Between days 25–78 post-

infection, Mtb burden continued to increase in both $VitD^{HI}$ and $VitD^{LO}$ groups albeit more slowly than days 1–25. At day 92 post-infection, we observed a modest increase in Mtb burden in $VitD^{HI}$ mice relative to $VitD^{LO}$ mice; however, this difference was directionally reversed by the last time point (day 110). Two-way ANOVA comparison of both $VitD^{LO}$ and $VitD^{HI}$ curves demonstrated that while the effect of time on bacterial burden was significant ($p<0.0001$), the effect of diet was not ($p = 0.1444$). Similarly, in the spleen – an organ to which Mtb disseminates 11–14 days post-infection in mice (43) – the effect of time was significant ($p<0.0001$) while no significant difference existed between the Mtb burdens of $VitD^{HI}$ and $VitD^{LO}$ groups ($p=0.6109$) (Fig 1C). Based on the growth characteristics of Mtb in $VitD^{LO}$ and $VitD^{HI}$ lungs, we termed post-infection days 1–40 as representing “early stage TB”, and the period thereafter as representing “late stage TB”; these terms are consistent with the terminology of others to describe the same periods (1, 4, 35). The abundance of bacteria in $VitD^{LO}$ and $VitD^{HI}$ mice during both early and late stage TB was also apparent by acid fast staining of lungs from these periods (Fig 1D–G). Collectively, these data demonstrate that dietary $VitD_3$ does not significantly affect bacterial burden during either early or late stages of experimental TB.

Dietary $VitD_3$ suppresses pro-inflammatory gene expression during late stage TB

Dietary $VitD_3$ has been repeatedly demonstrated to suppress organ-specific inflammation in autoimmune disease models (44). To determine if dietary $VitD_3$ limits pro-inflammatory gene expression in Mtb-infected organs, lungs from Mtb-infected $VitD^{LO}$ and $VitD^{HI}$ groups were collected on post-infection days 35 and 92, used for mRNA extraction and cDNA synthesis, and analyzed via real time PCR array for the expression of select genes of interest. Day 35 was chosen to represent early stage TB since, by this time, the adaptive immune response against Mtb has been established and limits Mtb growth (1); Day 92 was chosen to represent late stage TB. The results of this analysis are shown in Fig 2A and demonstrate that on post-infection day 35, the expression of multiple pro-inflammatory genes was increased in $VitD^{HI}$ lungs relative to $VitD^{LO}$ lungs. However by post-infection day 92, this difference in expression had inversed relative to that observed on post-infection day 35; namely, the expression pattern of many of the same genes was decreased in $VitD^{HI}$ lungs relative to $VitD^{LO}$ lungs. We confirmed this dynamic expression pattern for select genes of interest (e.g. *ifng*) by separate PCR (data not shown). In addition to the genes assessed via PCR array, we also compared $VitD^{LO}$ and $VitD^{HI}$ lungs’ expression of (Fig 2B) *cramp* (the mouse homolog of cathelicidin), (Fig 2C) *vdr* and (Fig 2D) *cyp27b1*. Cathelicidin is an effector of $VitD_3$-elicted Mtb growth restriction *in vitro* (24); VDR and CYP27b1 are essential for VitD3 signaling and metabolism, respectively. Our data demonstrate that *cramp* transcription was increased in both $VitD^{HI}$ and $VitD^{LO}$ groups following Mtb-infection (Fig 2B); the expression levels of *vdr* and *cyp27b1* varied with the timepoint examined, but did not significantly differ between $VitD^{HI}$ and $VitD^{LO}$ groups at each timepoint (Fig 2C–D). Therefore, any phenotypic differences between $VitD^{HI}$ and $VitD^{LO}$ mice are like not due to differences in VitD metabolism or antimicrobial peptide production.

To measure and compare the recall response in the spleens of Mtb-infected $VitD^{HI}$ and $VitD^{LO}$ mice, splenocytes were collected at 4 timepoints (post-infection days 1, 35, 62, 98), normalized for cell number and cultured in the presence of a polyclonal mitogen (ConA) and

3 different Mtb multiplicities of infection (MOI 0, 0.5 and 1). Two days later, culture supernatants were collected and used for ELISA measurements of both IL12/IL23p40 and IFNγ; macrophages and DCs are the principal sources of IL12/IL23p40 during experimental tuberculosis (6), while αβ T cells, NK cells, and neutrophils are the sources of IFNγ (5). The results of these recall experiments are shown in Fig 2E–F, and demonstrate that $VitD^{LO}$ splenocytes secreted significantly higher levels of IL12/IL23p40 and IFNγ on post-infection day 62 relative to $VitD^{HI}$ mice. This difference was observed at each MOI. Collectively, our lung transcription studies (Fig 2A) and splenocyte response studies (Fig 2E–F) demonstrate that dietary $VitD_3$ suppresses pro-inflammatory gene expression during late stage TB.

Dietary $VitD_3$ attenuates $CD3^+$ lymphocytes' contribution to lung granulomatous regions during late stage TB

The T_H1 response is required to limit TB, and manifests in Mtb-infected mouse lungs by the accumulation and organization of $CD3^+$ lymphocytes and innate myeloid-derived lineages (histiocytes) into granulomatous regions. To determine if dietary $VitD_3$ limits the manifestation of lung T_H1 immunity, we visually and quantitatively compared the contribution of $CD3^+$ lymphocytes to $VitD^{HI}$ and $VitD^{LO}$ lung granulomatous regions during early and late stage TB (Fig 3). Specifically, we used morphometric analysis of sections stained with hematoxylin/eosin (H&E) and CD3-specific monoclonal antibody (IHC) to determine the area of each granulomatous region and the extent to which lymphocytes contributed to each granulomatous region (Supplemental Fig 1); 4 sections per lung were analyzed in this manner, with each section containing 2–3 distinct granulomatous regions. H&E stains of representative granulomatous regions from $VitD^{LO}$ and $VitD^{HI}$ mice are shown in Fig 3A and Fig 3B, respectively; shown in each row are successively higher magnifications (4×, 10×, 20× and 100×) demonstrating that hematoxylin rich areas primarily comprise cells with lymphocyte morphology (small cells with a large nucleus:cytoplasm ratio). IHC on $VitD^{LO}$ lungs (Fig 3C) and $VitD^{HI}$ lungs (Fig 3D) demonstrated these lymphocytes to be highly reactive with anti-CD3. The average area of $VitD^{LO}$ and $VitD^{HI}$ granulomatous regions were similar during late stage TB (Fig 3G). However, a notable difference between $VitD^{LO}$ and $VitD^{HI}$ mice was that the extent to which lymphocytes contributed to each granuloma area was significantly lower in $VitD^{HI}$ mice relative to $VitD^{LO}$ mice during late stage TB; this difference was both visually apparent (compare the sizes of the hematoxylin staining regions in Fig 3A to those of Fig 3B) and quantifiable (Fig 3H). Regarding the extent to which these lymphocytes were $CD3^+$, digital IHC quantification (Supplemental Fig 2) demonstrated that during early stage TB, $VitD^{HI}$ mice had a greater frequency of $CD3^+$ lymphocytes in the lung; this difference did not exist during late stage TB. These $CD3^+$ cells most likely represent effector lineages, as Foxp3 IHC (Fig 3E–F) and digital Foxp3 IHC analysis (Fig 3J) demonstrate low frequencies of $Foxp3^+$ cells in the granulomatous regions of both $VitD^{LO}$ and $VitD^{HI}$ lungs. Collectively, these data demonstrate that dietary $VitD_3$ attenuates $CD3^+$ lymphocytes' contribution to Mtb granulomatous regions.

Dietary $VitD_3$ limits the accumulation of T_H1 cells during experimental TB

To characterize the T cells that develop in $VitD^{HI}$ and $VitD^{LO}$ mice following Mtb-infection, mediastinal lymph nodes (MLNs) of Mtb-infected $VitD^{LO}$ and $VitD^{HI}$ mice were removed

on days 25, 35 and 92 post-infection and used for flow cytometric analysis of CD4, CD8, IFNγ and TNFα staining. For reference purposes, MLN preparations from Mtb-infected $VitD^{STD}$ mice were analyzed in an identical manner. The results of this analysis are shown in Fig 4, and demonstrate that on day 25 post-infection, MLN preparations of both groups comprised roughly equal frequencies of $CD4^+$ and $CD8^+$ cells (Fig 4A, E–F). By post-infection days 35 and 92, the frequency of $CD4^+$ cells had grown more prominent in both groups, albeit significantly higher in $VitD^{LO}$ mice compared to $VitD^{HI}$ mice (Fig 4B–C, E); MLN $CD8^+$ frequencies were also higher in $VitD^{LO}$ mice on post-infection day 92 (Fig 4C, F). Regarding MLN cells' capacity to produce cytokines, $VitD^{HI}$ $CD4^+$ cells displayed a greater capacity to produce IFNγ on days 25 and 35 (Fig 4G); by day 92, the frequency of $CD4^+IFN\gamma^+$ cells in $VitD^{HI}$ and $VitD^{LO}$ mice were equal (Fig 4G). At all timepoints, the frequency of $CD4^+TNF\alpha^+$, $CD8^+IFN\gamma^+$ and $CD8^+TNF\alpha^+$ cells were similar between $VitD^{HI}$ and $VitD^{LO}$ groups (Fig 4H–J). Collectively, these data demonstrate that dietary $VitD_3$ limits the accumulation of IFNγ- and TNFα-producing $CD4^+$ (i.e. T_H1) cells during experimental TB.

Dietary $VitD_3$ alters the representation of $F4/80^+$ and $Ly6C/Ly6G^+$ lineages in lung granulomatous regions

That the granulomatous regions of $VitD^{HI}$ mice contained fewer $CD3^+$ lymphocytes, but were nevertheless equal in size to the granulomatous regions of $VitD^{LO}$ mice raised the question of whether histiocyte and/or polymorphonuclear lineages were over-represented in $VitD^{HI}$ granulomatous regions. To address this question, lung sections serial to those shown in Fig 4C–D were stained with antibodies specific to F4/80 and Ly6C/Ly6G. In Mtb-infected C3HeB/FeJ mice, F4/80 is a marker of both macrophages and myeloid derived suppressor cells (MDSCs), while Ly6C/Ly6G is a marker of both neutrophils and MDSCs (45). Representative F4/80 staining from both days 35 and 92 are shown in Figs 5A–D, along with quantitation of the same images in Fig 5E; representative Ly6C/Ly6G staining from both days 35 and 92 are shown in Figs 5F–I, along with quantitation of the same images in Fig 5J. Visual and quantitative analysis was limited to granulomatous regions; uninvolved lung regions were excluded from our analysis. The data demonstrate on post-infection day 35, the representation of both $F4/80^+$ and $Ly6C/Ly6G^+$ histiocytes was higher in $VitD^{HI}$ granulomas relative to $VitD^{LO}$ granulomas (Fig 5E,J). The elevated representation of $F4/80^+$ histiocytes in $VitD^{HI}$ granulomas continued to post-infection day 92 (Fig 5E). Collectively, these data demonstrate that dietary $VitD_3$ accelerating the accumulation of $F4/80^+$ and $Ly6C/Ly6G^+$ lineages during experimental TB.

Dietary $VitD_3$ suppresses pulmonary immunopathology during late stage TB

A negative consequence of inflammation in the Mtb-infected lung is immunopathology (8, 9, 46, 47). Given our observation that dietary $VitD_3$ limits the inflammatory response in Mtb-infected lung and spleen, we wished to determine if $VitD^{HI}$ mice were protected from Mtb-associated lung pathology. In C3HeB/FeJ mice and other TB-susceptible mouse strains, the progression of lung pathology associated with the appearance of acid fast bacilli (AFB) in acellular areas of lung granulomatous regions (34). The acellular areas of granulomatous regions are a consequence of necrosis, and are enriched in fragmented nuclei and membrane cholesterol (48). On day 35 post-infection, AFB were readily apparent in the granulomatous

regions of $VitD^{LO}$ mice (Fig 1C) and $VitD^{HI}$ mice (Fig 1E); in neither group were AFB found outside of the granuloma at this timepoint. By day 92 post-infection, AFB were found to associate with foamy macrophages in both $VitD^{LO}$ mice (Fig 1D) and $VitD^{HI}$ mice (Fig 1F). However, primarily in $VitD^{LO}$ granulomas (post-infection day 92) we also observed acellular areas with abundant AFB (Fig 6A, B). These acellular areas were characterized by the appearance of lipid droplets in which AFB could occasionally be found within (Fig 6A) and cholesterol clefts to which AFB were consistently in proximity (Fig 6B). Quantitative analysis confirmed $VitD^{LO}$ lung sections contained significantly more cholesterol clefts than $VitD^{HI}$ lungs (Fig 6C). Additional examination of $VitD^{LO}$ granulomas demonstrated that fragmented nuclei were also present in these acellular regions, as evidenced by hematoxylin-staining puncta (Fig 6D); acid-fast staining demonstrated AFB were often in close proximity to these fragmented nuclei (Fig 6E). Finally, when cholesterol cleft-containing regions of the lung were stained with either F4/80 or Ly6C/Ly6G, we observed that cholesterol clefts were consistently surrounded by Ly6C/Ly6G-staining tissue (Fig 6F–H); only occasionally did F4/80 staining associate with cholesterol clefts (data not shown). Collectively, these data demonstrate that dietary $VitD_3$ suppresses pulmonary immunopathology during late stage TB.

Hematopoietic VitD-responsiveness is required to limit TB immunopathology

There are several distinct lineages within an Mtb-infected animal that are responsive to VitD: host hematopoietic cells, host non-hematopoietic cells, the microbiome and Mtb itself. To determine if host cells must be VitD-responsive to limit TB-associated immunopathology, we aerosol-infected $vdr^{-/-}$ mice and compared the lung immunopathology that subsequently developed to that observed in C57BL/6 controls. *vdr* encodes the Vitamin D Receptor that is necessary for VitD-responsiveness (36); when placed on a “rescue diet” containing excess lactose, $vdr^{-/-}$ mice are nearly indistinguishable from $vdr^{+/+}$ mice in terms of hematopoietic and non-hematopoietic development (40–42). Analogous to our experiments with C3HeB/FeJ mice, $vdr^{+/+}$ and $vdr^{-/-}$ mice were placed on a rescue diet containing high levels of VitD for one month prior to Mtb-infection, and were kept on the same diet throughout the experiment timecourse; at indicated times, the lungs were removed and used for an analysis of Mtb burden and lung immunopathology.

Consistent with our studies of $VitD^{LO}$ and $VitD^{HI}$ C3HeB/FeJ mice, neither lung (Fig 7A) nor spleen (Fig 7B) Mtb-burdens differed between $vdr^{+/+}$ and $vdr^{-/-}$ mice. However, upon visual examination of Mtb-infected $vdr^{+/+}$ and $vdr^{-/-}$ lungs, we noted a greater representation of lymphocytes in $vdr^{-/-}$ granulomas, and that the histiocyte-rich regions of $vdr^{-/-}$ granulomas also showed evidence of necrosis (Fig 7C–D). Specifically, picnotic and karyorrhectic nuclei were abundant in histiocyte-rich regions (compare Fig 7Ci to Fig 7Di), and parenchyma destruction was also occasionally observed (Fig 7Dii). To quantify these histological differences, and to determine if these features were due to *vdr*-deficiency in hematopoietic or non-hematopoietic lineages, we generated and infected radiation bone marrow chimeras in which *vdr*-deficiency was restricted to either the hematopoietic compartment (i.e. donor $vdr^{-/-} \rightarrow vdr^{+/+}$ hosts) or non-hematopoietic compartment (i.e. donor $vdr^{+/+} \rightarrow vdr^{-/-}$ hosts); $vdr^{+/+} \rightarrow vdr^{+/+}$ and $vdr^{-/-} \rightarrow vdr^{-/-}$ radiation bone marrow chimeras were also generated and used as controls. As shown in Figure 7E–H, despite each

group having equivalent Mtb burdens (Fig 7E–F), $vdr^{-/-} \rightarrow vdr^{+/+}$ and $vdr^{-/-} \rightarrow vdr^{-/-}$ lungs displayed higher levels of immunopathology as measured by the increased representation of lymphocytes (Fig 7G) and picnotic or karyorrhectic nuclei (Fig 7H) within their granulomatous regions. These characteristics did not appear in uninfected $vdr^{-/-} \rightarrow vdr^{+/+}$ controls (data not shown). Collectively, these data demonstrate that hematopoietic responses to VitD are required to limit TB immunopathology.

DISCUSSION

Despite there having been longstanding interest in $VitD_3$ as an adjunctive therapy for TB (49), there have until now been no *in vivo* studies of $VitD_3$'s effect on the pulmonary immune response to Mtb. This represents a significant gap in the TB immunology research continuum. To fill this gap, we used C3HeB/FeJ mice fed diets either deficient or replete with $VitD_3$ and aerosol infected them with virulent Mtb. At timepoints representing early and late stage TB, both groups were examined for changes in VitD status and metabolism, as well as standard experimental TB readouts. Our results demonstrate that dietary $VitD_3$ modulates the pulmonary immune response by altering the accumulation dynamics of $CD3^+$ lymphocytes, and $F4/80^+$ and $Ly6C/Ly6G^+$ histiocytes in granulomatous regions; the overall consequence of these changes is a microenvironment that suppresses immunopathology while still permitting Mtb control. Collectively, our data support a model wherein VitD is acting *in vivo* during TB not as a bactericide, but rather as an immunosuppressant that limits pulmonary inflammation to levels that are sufficient to control Mtb but limited in the ability to cause pathology.

$VitD_3$ is well-recognized in many areas of immunology research as having immunosuppressive activity (44). However, in the field of TB Immunology, the prevailing model of how VitD affects TB has until this point centered around VitD's direct and indirect mycobactericidal activities (25). VitD's direct mycobactericidal activity in Mtb broth culture has been repeatedly demonstrated (20, 21). The indirect mycobactericidal activity of VitD has also been repeatedly demonstrated using co-cultures of primary human MØs and virulent Mtb, a system in which VitD synergizes with IFNγ to increase production of cathelicidin (23, 24) - an antimicrobial peptide which is cytotoxic in Mtb broth cultures (26). At the patient level, there is an inverse correlation between circulating 25(OH)D concentrations and risk of both active and latent TB (27, 50, 51). However, clinical trials testing $VitD_3$'s utility as an adjunctive therapy for TB have failed to produce striking changes in sputum conversion rate, despite involving hundreds of individuals and independent statistical analyses (27–30). We propose that rather than serving to enhance killing of Mtb, VitD instead protects the host by limiting Mtb-elicited inflammation. Put in terms of the "disease tolerance" framework (9), VitD reduces the fitness cost of Mtb infection by promoting tolerance (i.e. reducing the negative impact of infection) instead of promoting resistance (i.e. reducing pathogen burden once an infection is established).

The appropriateness of mice as a model organism for studies of TB pathology has been a subject of deliberation for several years (52). One reason for this is that the granulomas that develop in common mouse strains (e.g. C57BL/6, BALB/c) do not, as a general rule, display caseous necrosis (34) - a defining feature of granulomas in untreated human TB (53). While

there are exceptions to this general rule (47), the infrequency of caseous necrosis in common strains makes it difficult to systematically determine the biology underlying formation of necrotic lesions. For this reason, the development of the C3HeB/FeJ model by Kramnik and colleagues (54) was a major step forward for the field, as mice permit investigations that otherwise can not be performed in other animal models for either technical or economic reasons. Relative to C57BL/6 mice, Mtb infected C3HeB/FeJ mice have been reported to die more quickly, have accelerated Mtb growth in the lung and spleen, and develop necrotic caseous lung lesions (54). Contrasting with these previous studies, none of the C3HeB/FeJ mice in our study developed the large caseous lesions, high Mtb burdens (~10^{8-9} CFU), and mortality reported to develop in C3HeB/FeJ mice by ~30 days post-infection (54). Instead, we found the Mtb growth characteristics in C3HeB/FeJ mice to resemble those historically observed in C57BL/6 mice (52). Nevertheless, the immunopathology we observed in C3HeB/FeJ mice was more severe than any we have ever seen in C57BL/6 mice (5, 6). Specifically, we observed necrotic areas in H37Rv-infected $VitD^{LO}$ mice during late stage TB that contained abundant AFB. The reason we did not observe the caseous lesions reported by others is unknown at this time, but likely relates to the use of different Mtb strains (Erdman vs. H37Rv) or passaging protocols (55). It is also possible that more dramatic differences in either Mtb burden, immunopathology or mRNA expression readouts occur between $VitD^{LO}$ and $VitD^{HI}$ mice at other timepoints, including the period between post-infection days 35 and 92.

Regarding the mechanism by which VitD functions through hematopoietic cells to suppress TB, there are two possibilities that are the subject of future investigations in our lab. First, given transgenic *Ipr1*'s ability to suppress pathology in C3HeB/FeJ mice (56), it is possible that VitD increases the bioactivity of *Ipr1* in Mtb-infected MØs. In terms of basic *Ipr1* biology, little is known about Ipr1 other than it is an IFN-inducible nuclear protein that switches MØ programming from necrosis to apoptosis. Second, despite Foxp3 staining being similar in $VitD^{LO}$ and $VitD^{HI}$ granulomatous regions, it remains possible that dietary $VitD_3$ elicits regulatory T cells (T_{REGs}) that are more capable of suppressing lung immunopathology. T_{REGs} develop early following mouse Mtb-infection, and delay the onset of T_H1 immunity (4). Although T_{REGs}' role in limiting TB immunopathology is suggested by comparing lung T_{REG} numbers in TB-resistant and TB-susceptible mouse strains (57), this role has not yet been empirically tested.

Finally, we believe it is important to relate the findings of the present study to that of the human clinical trial data reported by Martineau and colleagues (27, 58). Martineau et al (27) demonstrated that although administering adjunct $VitD_3$ increases serum 25(OH)D levels in patients receiving treatment for pulmonary TB, it does not significantly affect time to sputum culture conversion. When their results were stratified based on participants *Taq*I genotype (a silent polymorphism in VDR exon 9), a modest reduction in time to sputum culture conversion was observed in patients with the *tt* genotype relative to those with either the *TT* or *Tt* genotype. Individuals with the *tt* genotype comprise <9% of populations most effected by TB (59). Among the same study participants, Coussens et al (58) observed a more profound effect of adjunct $VitD_3$: namely, $VitD_3$ supplementation reduced markers of systemic inflammation in humans during TB treatment. Specifically, PBMCs from $VitD_3$-treated TB patients produced less IL1R1A, IL6, IL12 and TNFα following *ex vivo*

stimulation with Mtb CFP-10 (relative to PBMCs from placebo-treated TB patients). Adjunctive $VitD_3$ also lowered the monocyte:lymphocyte balance in the circulation of TB patients; a high monocyte:lymphocyte ratio associates with increased disease hazards in some TB patient subpopulations (60–62). Also, and contrary to what Coussens et al expected based on previous literature, adjunct $VitD_3$ suppressed circulating cathelicidin levels in TB patients (58). Our Mtb-infected $VitD^{HI}$ mice phenocopy the $VitD_3$-treated TB patients of Coussens et al in the following ways: VitD reduced pulmonary expression of IL1r1, IL6, TNFα (Fig 2a); VitD reduced splenocyte IL12/23p40-secretion following ex vivo stimulation (Fig 2E); VitD reduced the frequency of lymphocytes in the lung granuloma and draining lymph node (Figs 3H, 4D–E); VitD affected neither Mtb burden nor cathelicidin-related antimicrobial peptide expression.

After considering the clinical trial data of Coussens et al (58) alongside the findings of the present study, we propose that in most individuals VitD does not function to enhance Mtb-killing in the manner advocated by Modlin and Bloom (25). Instead, VitD protects the host by reducing Mtb-elicited inflammation to a level that is still sufficient to restrict Mtb growth but unable to cause pathology. Although the model of VitD being bactericidal is firmly rooted in reviews of TB literature, the alternative model of VitD being a suppressor of TB immunopathology is already being promoted (63). Our study supports this alternative view of the VitD-TB interaction. Our study also illustrates that a small animal model can be used to advance the understanding of an effect that has been demonstrated in a human clinical trial (that vitamin D supplementation modulates inflammatory responses in TB). This is important given recent concerns that small animal TB models misled development of MVA85A, a new tuberculosis vaccine that was ultimately non-efficacious in human infants (64). As future clinical trials are designed to investigate $VitD_3$ as an adjunct therapy for TB – as well as TB associated immune reconstitution inflammatory syndrome (IRIS) – it behooves us to move beyond traditional readouts of success (i.e. reduced time to sputum conversion) to also consider reductions in lung pathology and individual morbidity as successful outcomes (63).

Supplementary Material

Refer to Web version on PubMed Central for supplementary material.

Acknowledgments

We would like to acknowledge and thank Drs. Paula North, Suresh Kumar of the Children's Hospital of Wisconsin Histology Core for their assistance in our histological analysis, and Dr. Aniko Szabo of the MCW Biostatistics Consulting Service for her assistance with our statistical analysis.

This study was supported by the Medical College of Wisconsin (MCW), the MCW Center for Infectious Disease Research (CIDR), Advancing a Healthier Wisconsin grant 5520189, a BD Biosciences Immunology Grant, and the National Institutes of Health (R21AI099661 to R.T.R.).

References

1. Cooper AM. Cell-mediated immune responses in tuberculosis. Annu Rev Immunol. 2009; 27:393–422. [PubMed: 19302046]

2. World Health Organization. Global Tuberculosis Report. 2015. http://www.who.int/tb/publications/global_report/en/
3. Dye C, Glaziou P, Floyd K, Raviglione M. Prospects for tuberculosis elimination. Annu Rev Public Health. 2013; 34:271–286. [PubMed: 23244049]
4. Urdahl KB. Understanding and overcoming the barriers to T cell-mediated immunity against tuberculosis. Semin Immunol. 2014; 26:578–587. [PubMed: 25453230]
5. Miller HE, Robinson RT. Early control of Mycobacterium tuberculosis infection requires il12rb1 expression by rag1-dependent lineages. Infect Immun. 2012; 80:3828–3841. [PubMed: 22907814]
6. Reeme AE, Miller HE, Robinson RT. IL12B expression is sustained by a heterogenous population of myeloid lineages during tuberculosis. Tuberculosis (Edinb). 2013; 93:343–356. [PubMed: 23491716]
7. Green AM, Difazio R, Flynn JL. IFN-gamma from CD4 T cells is essential for host survival and enhances CD8 T cell function during Mycobacterium tuberculosis infection. J Immunol. 2013; 190:270–277. [PubMed: 23233724]
8. Achkar JM, Jenny-Avital ER. Incipient and subclinical tuberculosis: defining early disease states in the context of host immune response. J Infect Dis. 2011; 204(Suppl 4):S1179–1186. [PubMed: 21996700]
9. Medzhitov R, Schneider DS, Soares MP. Disease tolerance as a defense strategy. Science. 2012; 335:936–941. [PubMed: 22363001]
10. Holscher C, Holscher A, Ruckerl D, Yoshimoto T, Yoshida H, Mak T, Saris C, Ehlers S. The IL-27 receptor chain WSX-1 differentially regulates antibacterial immunity and survival during experimental tuberculosis. J Immunol. 2005; 174:3534–3544. [PubMed: 15749890]
11. Barber DL, Mayer-Barber KD, Feng CG, Sharpe AH, Sher A. CD4 T cells promote rather than control tuberculosis in the absence of PD-1-mediated inhibition. J Immunol. 2011; 186:1598–1607. [PubMed: 21172867]
12. Lazar-Molnar E, Chen B, Sweeney KA, Wang EJ, Liu W, Lin J, Porcelli SA, Almo SC, Nathenson SG, Jacobs WR Jr. Programmed death-1 (PD-1)-deficient mice are extraordinarily sensitive to tuberculosis. Proc Natl Acad Sci U S A. 2010; 107:13402–13407. [PubMed: 20624978]
13. Kiran D, Podell BK, Chambers M, Basaraba RJ. Host-directed therapy targeting the Mycobacterium tuberculosis granuloma: a review. Semin Immunopathol. 2015
14. Skerry C, Harper J, Klunk M, Bishai WR, Jain SK. Adjunctive TNF inhibition with standard treatment enhances bacterial clearance in a murine model of necrotic TB granulomas. PLoS One. 2012; 7:e39680. [PubMed: 22761866]
15. Tsenova L, Mangaliso B, Muller G, Chen Y, Freedman VH, Stirling D, Kaplan G. Use of IMiD3, a thalidomide analog, as an adjunct to therapy for experimental tuberculous meningitis. Antimicrob Agents Chemother. 2002; 46:1887–1895. [PubMed: 12019105]
16. Ralph AP, Lucas RM, Norval M. Vitamin D and solar ultraviolet radiation in the risk and treatment of tuberculosis. Lancet Infect Dis. 2013; 13:77–88. [PubMed: 23257233]
17. Bouillon R, Carmeliet G, Verlinden L, van Etten E, Verstuyf A, Luderer HF, Lieben L, Mathieu C, Demay M. Vitamin D and human health: lessons from vitamin D receptor null mice. Endocr Rev. 2008; 29:726–776. [PubMed: 18694980]
18. Esteban C, Geuskens M, Ena JM, Mishal Z, Macho A, Torres JM, Uriel J. Receptor-mediated uptake and processing of vitamin D-binding protein in human B-lymphoid cells. J Biol Chem. 1992; 267:10177–10183. [PubMed: 1374401]
19. Green M. Cod liver oil and tuberculosis. BMJ. 2011; 343:d7505. [PubMed: 22187324]
20. Greenstein RJ, Su L, Brown ST. Vitamins A & D inhibit the growth of mycobacteria in radiometric culture. PLoS One. 2012; 7:e29631. [PubMed: 22235314]
21. Crowle AJ, Salfinger M, May MH. 1,25(OH)2-vitamin D3 synergizes with pyrazinamide to kill tubercle bacilli in cultured human macrophages. Am Rev Respir Dis. 1989; 139:549–552. [PubMed: 2492412]
22. Liu PT, Stenger S, Li H, Wenzel L, Tan BH, Krutzik SR, Ochoa MT, Schauber J, Wu K, Meinken C, Kamen DL, Wagner M, Bals R, Steinmeyer A, Zugel U, Gallo RL, Eisenberg D, Hewison M, Hollis BW, Adams JS, Bloom BR, Modlin RL. Toll-like receptor triggering of a vitamin D-mediated human antimicrobial response. Science. 2006; 311:1770–1773. [PubMed: 16497887]

23. Fabri M, Stenger S, Shin DM, Yuk JM, Liu PT, Realegeno S, Lee HM, Krutzik SR, Schenk M, Sieling PA, Teles R, Montoya D, Iyer SS, Bruns H, Lewinsohn DM, Hollis BW, Hewison M, Adams JS, Steinmeyer A, Zugel U, Cheng G, Jo EK, Bloom BR, Modlin RL. Vitamin D is required for IFN-gamma-mediated antimicrobial activity of human macrophages. Sci Transl Med. 2011; 3:104ra102.
24. Liu PT, Stenger S, Tang DH, Modlin RL. Cutting edge: vitamin D-mediated human antimicrobial activity against Mycobacterium tuberculosis is dependent on the induction of cathelicidin. J Immunol. 2007; 179:2060–2063. [PubMed: 17675463]
25. Modlin RL, Bloom BR. TB or not TB: that is no longer the question. Sci Transl Med. 2013; 5:213sr216.
26. Castaneda-Delgado J, Hernandez-Pando R, Serrano CJ, Aguilar-Leon D, Leon-Contreras J, Rivas-Santiago C, Mendez R, Gonzalez-Curiel I, Enciso-Moreno A, Rivas-Santiago B. Kinetics and cellular sources of cathelicidin during the course of experimental latent tuberculous infection and progressive pulmonary tuberculosis. Clin Exp Immunol. 2010; 161:542–550. [PubMed: 20636399]
27. Martineau AR, Timms PM, Bothamley GH, Hanifa Y, Islam K, Claxton AP, Packe GE, Moore-Gillon JC, Darmalingam M, Davidson RN, Milburn HJ, Baker LV, Barker RD, Woodward NJ, Venton TR, Barnes KE, Mullett CJ, Coussens AK, Rutterford CM, Mein CA, Davies GR, Wilkinson RJ, Nikolayevskyy V, Drobniewski FA, Eldridge SM, Griffiths CJ. High-dose vitamin D(3) during intensive-phase antimicrobial treatment of pulmonary tuberculosis: a double-blind randomised controlled trial. Lancet. 2011; 377:242–250. [PubMed: 21215445]
28. Wejse C V, Gomes F, Rabna P, Gustafson P, Aaby P, Lisse IM, Andersen PL, Glerup H, Sodemann M. Vitamin D as supplementary treatment for tuberculosis: a double-blind, randomized, placebo-controlled trial. Am J Respir Crit Care Med. 2009; 179:843–850. [PubMed: 19179490]
29. Daley P, Jagannathan V, John KR, Sarojini J, Latha A, Vieth R, Suzana S, Jeyaseelan L, Christopher DJ, Smieja M, Mathai D. Adjunctive vitamin D for treatment of active tuberculosis in India: a randomised, double-blind, placebo-controlled trial. Lancet Infect Dis. 2015
30. Ralph AP, Waramori G, Pontororing GJ, Kenangalem E, Wiguna A, Tjitra E, Sandjaja, Lolong DB, Yeo TW, Chatfield MD, Soemanto RK, Bastian I, Lumb R, Maguire GP, Eisman J, Price RN, Morris PS, Kelly PM, Anstey NM. L-arginine and vitamin D adjunctive therapies in pulmonary tuberculosis: a randomised, double-blind, placebo-controlled trial. PLoS One. 2013; 8:e70032. [PubMed: 23967066]
31. Irwin SM, Gruppo V, Brooks E, Gilliland J, Scherman M, Reichlen MJ, Leistikow R, Kramnik I, Nuermberger EL, Voskuil MI, Lenaerts AJ. Limited activity of clofazimine as a single drug in a mouse model of tuberculosis exhibiting caseous necrotic granulomas. Antimicrob Agents Chemother. 2014; 58:4026–4034. [PubMed: 24798275]
32. Marzo E, Vilaplana C, Tapia G, Diaz J, Garcia V, Cardona PJ. Damaging role of neutrophilic infiltration in a mouse model of progressive tuberculosis. Tuberculosis (Edinb). 2014; 94:55–64. [PubMed: 24291066]
33. Apt A, Kramnik I. Man and mouse TB: contradictions and solutions. Tuberculosis (Edinb). 2009; 89:195–198. [PubMed: 19345146]
34. Driver ER, Ryan GJ, Hoff DR, Irwin SM, Basaraba RJ, Kramnik I, Lenaerts AJ. Evaluation of a mouse model of necrotic granuloma formation using C3HeB/FeJ mice for testing of drugs against Mycobacterium tuberculosis. Antimicrob Agents Chemother. 2012; 56:3181–3195. [PubMed: 22470120]
35. Harper J, Skerry C, Davis SL, Tasneen R, Weir M, Kramnik I, Bishai WR, Pomper MG, Nuermberger EL, Jain SK. Mouse model of necrotic tuberculosis granulomas develops hypoxic lesions. J Infect Dis. 2012; 205:595–602. [PubMed: 22198962]
36. Li YC, Pirro AE, Amling M, Delling G, Baron R, Bronson R, Demay MB. Targeted ablation of the vitamin D receptor: an animal model of vitamin D-dependent rickets type II with alopecia. Proc Natl Acad Sci U S A. 1997; 94:9831–9835. [PubMed: 9275211]
37. Rowling MJ, Gliniak C, Welsh J, Fleet JC. High dietary vitamin D prevents hypocalcemia and osteomalacia in CYP27B1 knockout mice. J Nutr. 2007; 137:2608–2615. [PubMed: 18029472]
38. Sergeev IN, Song Q. High vitamin D and calcium intakes reduce diet-induced obesity in mice by increasing adipose tissue apoptosis. Mol Nutr Food Res. 2014; 58:1342–1348. [PubMed: 24449427]

39. Meeker S, Seamons A, Paik J, Treuting PM, Brabb T, Grady WM, Maggio-Price L. Increased dietary vitamin D suppresses MAPK signaling, colitis, and colon cancer. Cancer Res. 2014; 74:4398–4408. [PubMed: 24938764]
40. Mathieu C, Van Etten E, Gysemans C, Decallonne B, Kato S, Laureys J, Depovere J, Valckx D, Verstuyf A, Bouillon R. In vitro and in vivo analysis of the immune system of vitamin D receptor knockout mice. J Bone Miner Res. 2001; 16:2057–2065. [PubMed: 11697802]
41. Mayne CG, Spanier JA, Relland LM, Williams CB, Hayes CE. 1,25-Dihydroxyvitamin D3 acts directly on the T lymphocyte vitamin D receptor to inhibit experimental autoimmune encephalomyelitis. Eur J Immunol. 2011; 41:822–832. [PubMed: 21287548]
42. Johnson LE, DeLuca HF. Vitamin D receptor null mutant mice fed high levels of calcium are fertile. J Nutr. 2001; 131:1787–1791. [PubMed: 11385068]
43. Chackerian AA, Alt JM, Perera TV, Dascher CC, Behar SM. Dissemination of Mycobacterium tuberculosis is influenced by host factors and precedes the initiation of T-cell immunity. Infect Immun. 2002; 70:4501–4509. [PubMed: 12117962]
44. Hayes CE, Hubler SL, Moore JR, Barta LE, Praska CE, Nashold FE. Vitamin D Actions on CD4(+) T Cells in Autoimmune Disease. Front Immunol. 2015; 6:100. [PubMed: 25852682]
45. Obregon-Henao A, Henao-Tamayo M, Orme IM, Ordway DJ. Gr1(int)CD11b+ myeloid-derived suppressor cells in Mycobacterium tuberculosis infection. PLoS One. 2013; 8:e80669. [PubMed: 24224058]
46. Casadevall A, Pirofski LA. The damage-response framework of microbial pathogenesis. Nat Rev Microbiol. 2003; 1:17–24. [PubMed: 15040176]
47. Hunter RL, Jagannath C, Actor JK. Pathology of postprimary tuberculosis in humans and mice: contradiction of long-held beliefs. Tuberculosis (Edinb). 2007; 87:267–278. [PubMed: 17369095]
48. Orme IM, Basaraba RJ. The formation of the granuloma in tuberculosis infection. Semin Immunol. 2014; 26:601–609. [PubMed: 25453231]
49. Ellman P, Anderson KH. Calciferol in tuberculous peritonitis with disseminated tuberculosis. Br Med J. 1948; 1:394. [PubMed: 18905261]
50. Nielsen NO, Skifte T, Andersson M, Wohlfahrt J, Soborg B, Koch A, Melbye M, Ladefoged K. Both high and low serum vitamin D concentrations are associated with tuberculosis: a case-control study in Greenland. Br J Nutr. 2010; 104:1487–1491. [PubMed: 20553638]
51. Gibney KB, MacGregor L, Leder K, Torresi J, Marshall C, Ebeling PR, Biggs BA. Vitamin D deficiency is associated with tuberculosis and latent tuberculosis infection in immigrants from sub-Saharan Africa. Clin Infect Dis. 2008; 46:443–446. [PubMed: 18173355]
52. Flynn JL. Lessons from experimental Mycobacterium tuberculosis infections. Microbes Infect. 2006; 8:1179–1188. [PubMed: 16513383]
53. Hunter RL. Pathology of post primary tuberculosis of the lung: an illustrated critical review. Tuberculosis (Edinb). 2011; 91:497–509. [PubMed: 21733755]
54. Kramnik I, Dietrich WF, Demant P, Bloom BR. Genetic control of resistance to experimental infection with virulent Mycobacterium tuberculosis. Proc Natl Acad Sci U S A. 2000; 97:8560–8565. [PubMed: 10890913]
55. Dietrich J, Roy S, Rosenkrands I, Lindenstrom T, Filskov J, Rasmussen EM, Cassidy J, Andersen P. Differential influence of nutrient starved Mycobacterium tuberculosis on adaptive immunity results in progressive TB disease and pathology. Infect Immun. 2015
56. Pan H, Yan BS, Rojas M, Shebzukhov YV, Zhou H, Kobzik L, Higgins DE, Daly MJ, Bloom BR, Kramnik I. Ipr1 gene mediates innate immunity to tuberculosis. Nature. 2005; 434:767–772. [PubMed: 15815631]
57. Leepiyasakulchai C, Ignatowicz L, Pawlowski A, Kallenius G, Skold M. Failure to recruit anti-inflammatory CD103+ dendritic cells and a diminished CD4+ Foxp3+ regulatory T cell pool in mice that display excessive lung inflammation and increased susceptibility to Mycobacterium tuberculosis. Infect Immun. 2012; 80:1128–1139. [PubMed: 22215739]
58. Coussens AK, Wilkinson RJ, Hanifa Y, Nikolayevskyy V, Elkington PT, Islam K, Timms PM, Venton TR, Bothamley GH, Packe GE, Darmalingam M, Davidson RN, Milburn HJ, Baker LV, Barker RD, Mein CA, Bhaw-Rosun L, Nuamah R, Young DB, Drobniewski FA, Griffiths CJ,

Martineau AR. Vitamin D accelerates resolution of inflammatory responses during tuberculosis treatment. Proc Natl Acad Sci U S A. 2012; 109:15449–15454. [PubMed: 22949664]

59. Chen C, Liu Q, Zhu L, Yang H, Lu W. Vitamin D receptor gene polymorphisms on the risk of tuberculosis, a meta-analysis of 29 case-control studies. PLoS One. 2013; 8:e83843. [PubMed: 24349552]
60. Naranbhai V, Hill AV, Abdool Karim SS, Naidoo K, Abdool Karim Q, Warimwe GM, McShane H, Fletcher H. Ratio of monocytes to lymphocytes in peripheral blood identifies adults at risk of incident tuberculosis among HIV-infected adults initiating antiretroviral therapy. J Infect Dis. 2014; 209:500–509. [PubMed: 24041796]
61. Naranbhai V, Kim S, Fletcher H, Cotton MF, Violari A, Mitchell C, Nachman S, McSherry G, McShane H, Hill AV, Madhi SA. The association between the ratio of monocytes:lymphocytes at age 3 months and risk of tuberculosis (TB) in the first two years of life. BMC Med. 2014; 12:120. [PubMed: 25034889]
62. Naranbhai V, Moodley D, Chipato T, Stranix-Chibanda L, Nakabaiito C, Kamateeka M, Musoke P, Manji K, George K, Emel LM, Richardson P, Andrew P, Fowler M, Fletcher H, McShane H, Coovadia HM, Hill AV. The association between the ratio of monocytes: lymphocytes and risk of tuberculosis among HIV-infected postpartum women. J Acquir Immune Defic Syndr. 2014; 67:573–575. [PubMed: 25247435]
63. Coussens AK, Martineau AR, Wilkinson RJ. Anti-Inflammatory and Antimicrobial Actions of Vitamin D in Combating TB/HIV. Scientifica (Cairo). 2014:903680. [PubMed: 25101194]
64. Tameris MD, Hatherill M, Landry BS, Scriba TJ, Snowden MA, Lockhart S, Shea JE, McClain JB, Hussey GD, Hanekom WA, Mahomed H, McShane H. Safety and efficacy of MVA85A, a new tuberculosis vaccine, in infants previously vaccinated with BCG: a randomised, placebo-controlled phase 2b trial. Lancet. 2013; 381:1021–1028. [PubMed: 23391465]

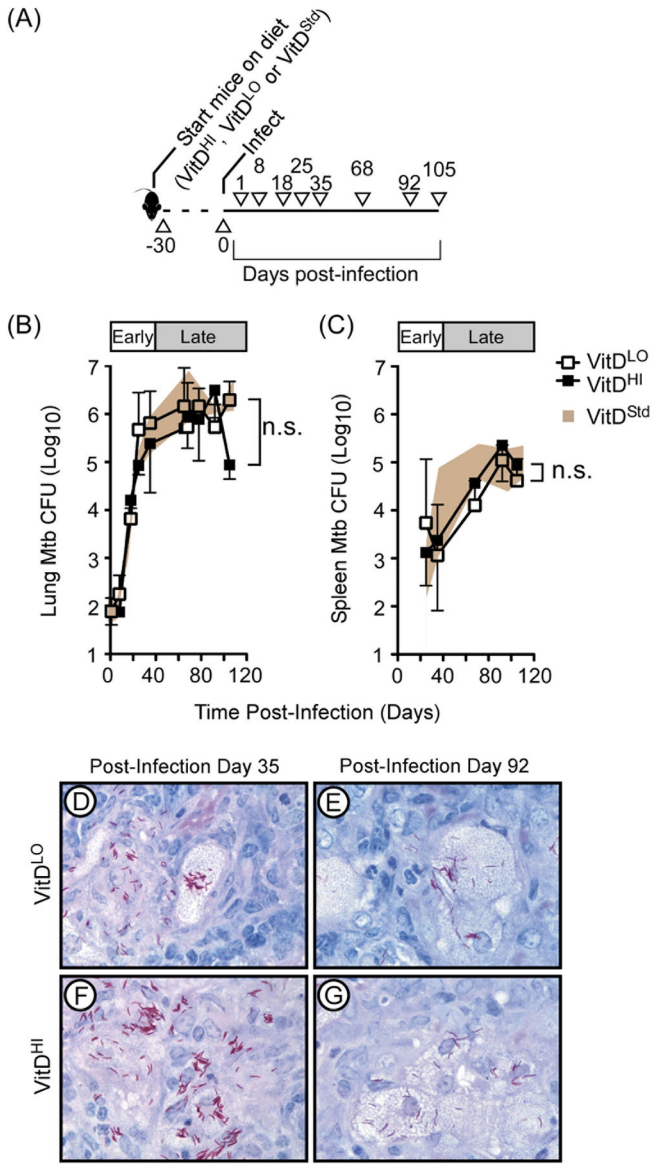

FIGURE 1. Dietary $VitD_3$ does not significantly affect bacterial burden in lung and spleen during experimental TB

(**A**) Our experimental setup is depicted. $VitD^{Std}$, $VitD^{HI}$ and $VitD^{LO}$ mice were aerosol infected with 46–108 Mtb H37Rv (day 0) and experimental readouts measured on indicated days. (**B–C**) Shown are the mean CFU burdens (±SD) in the (**B**) lungs and (**C**) spleens of $VitD^{HI}$ and $VitD^{LO}$ groups (closed squares, $VitD^{HI}$; open squares, $VitD^{LO}$). The brown shaded area in (**B–C**) represents the CFU value standard deviation in infected $VitD^{Std}$ mice over the same timecourse. Two-way ANOVA analysis demonstrated that the effect of diet on either lung or spleen CFU burden was not significant (p= 0.1444, lung; p= 0.6109, spleen). (**D–G**) Representative images demonstrating the localization of AFB in granulomatous regions on (**D, F**) post-infection day 35 and (**E, G**) post-infection day 92 in both groups. This experiment was repeated twice, each with similar results (3–4 mice/group/timepoint); n.s., not significant.

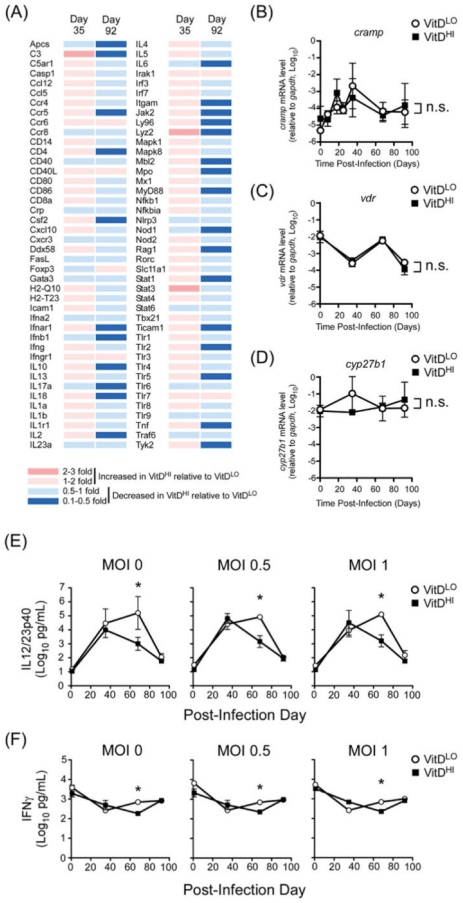

FIGURE 2. Dietary VitD$_3$ suppresses pro-inflammatory gene expression during late stage TB

(**A**) On post-infection days 35 and 92, lungs from VitD^{LO} and VitD^{HI} groups (3–4 mice per group) were collected and used for PCR array analysis of genes associated with innate and adaptive immunity. Shown in heat map format is the expression of each gene in VitD^{HI} lungs relative to VitD^{LO} lungs at both time points ($\Delta\Delta C_t$). Next to each gene abbreviation are data from post-infection day 35 (leftmost column) and post-infection day 92 (rightmost column); the legend at the bottom indicates the fold change corresponding to each color (red, increased in VitD^{HI} mice relative to VitD^{LO} mice; blue, decreased in VitD^{HI} mice relative to VitD^{LO} mice). (**B–D**) For both VitD^{LO} and VitD^{HI} groups, quantitative real time PCR analysis was used to measure (**B**) *cramp*, (**C**) *vdr* and (**D**) *cyp27b1* expression relative to *gapdh* at indicated timepoints Each data point indicates the mean expression level ±SD for each gene at each timepoint. (**E–F**) Following *in vitro* restimulation of splenocytes from Mtb-infected VitD^{HI} and VitD^{LO} mice, supernatants were collected and used for ELISA analysis of (**E**) IL12/IL23p40 levels and (**F**) IFNγ levels. For both (**B–D**) gene expression studies and (**E–F**) cytokine production studies, two-way ANOVA analysis was used to determine statistical significance; *, $p \leq 0.05$.

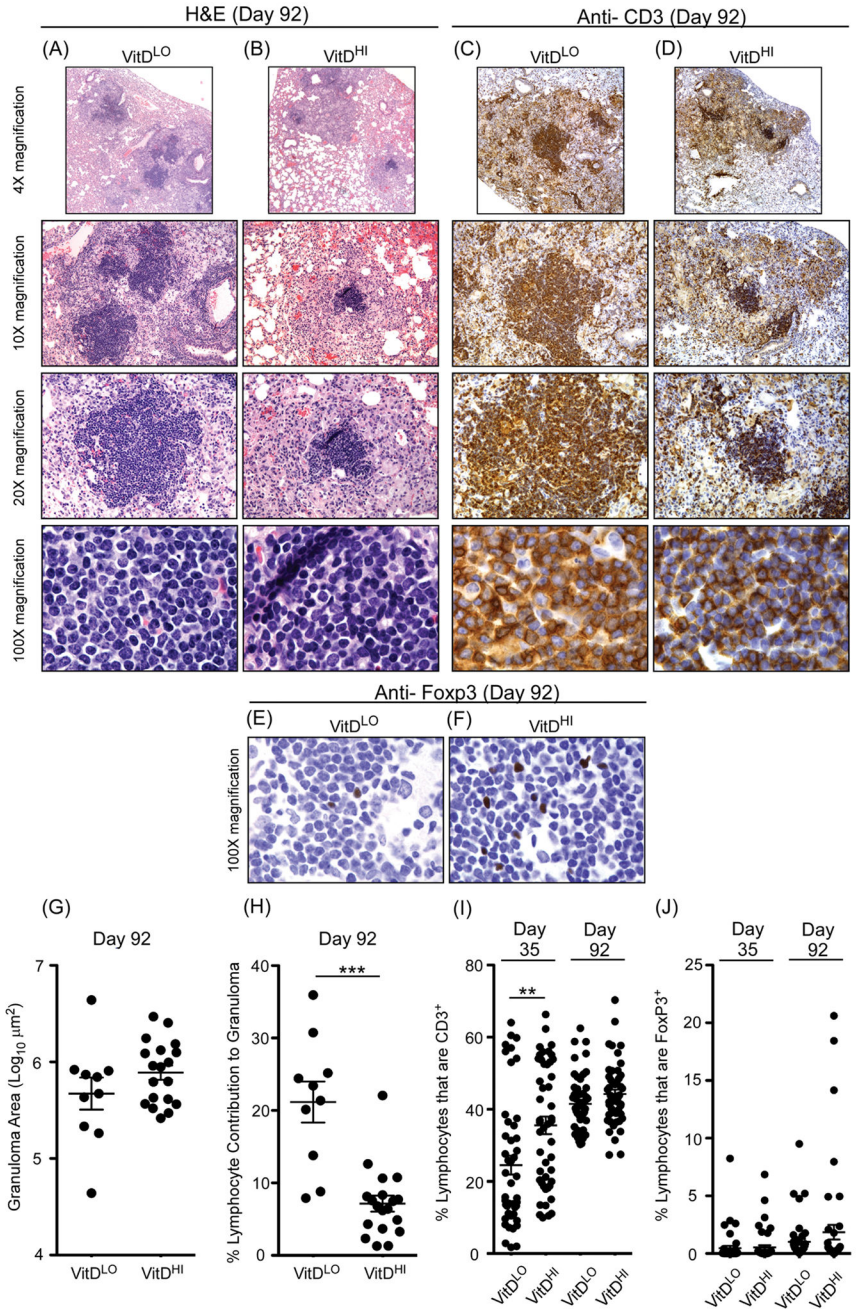

FIGURE 3. Dietary $VitD_3$ attenuates $CD3^+$ lymphocytes' contribution to granulomatous regions during late stage TB

Lung sections from (**A,C**) $VitD^{LO}$ mice and (**B,D**) $VitD^{HI}$ mice were stained with either (**A,B**) H&E (purple, nuclei; pink, protein) or (**C,D**) anti-CD3 IHC (brown, CD3; blue, nuclei). Shown are **(A–D)** representative granulomatous regions in each group on post-infection day 92 at 4× magnification (first row), 10× magnification (second row), 20× magnification (third row) and 100× magnification (fourth row). Also shown at 100x magnification are (**E–F**) representative Foxp3 IHC stains of lungs from the same groups. (**G–H**) H&E stained sections from mice at post-infection day 92 were used for

morphometric measurement of (**G**) the total area of each granulomatous region in each group and (**H**) the extent to which lymphocytes contributed to the area of each granulomatous region. (**I–J**) For both $VitD^{LO}$ and $VitD^{HI}$ lungs, digital IHC analysis was used to determine the percent of lymphocytes expressing (**I**) CD3 or (**J**) Foxp3 on post-infection days 35 and 92. Each data point in (**I–J**) represents the frequency of positive cells in one 20x region of interest (ROI) within an individual granuloma; ~50 ROI per group (4 mice/group) were analyzed in this manner. **, $p \leq 0.005$ and ***, $p \leq 0.0005$ as determined by Student's t-test.

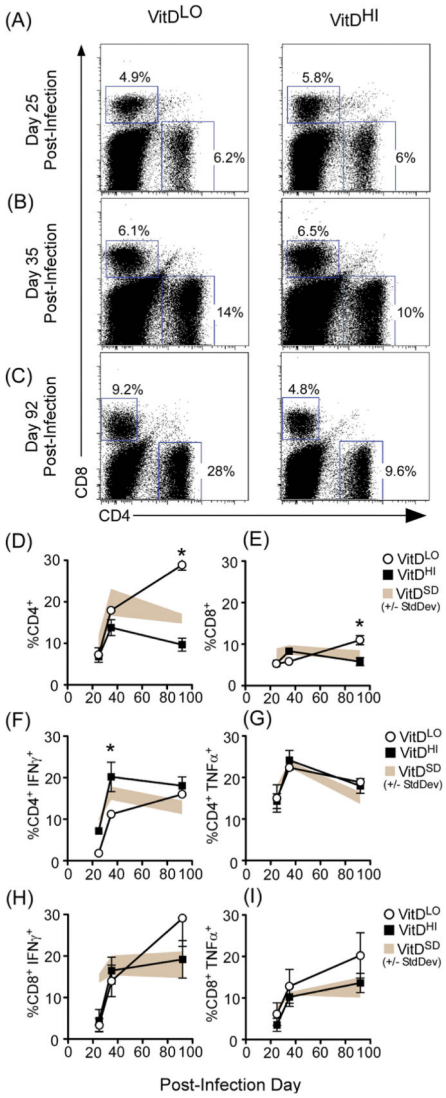

FIGURE 4. Dietary VitD$_3$ limits the accumulation of T$_H$1 cells during experimental TB

MLNs from Mtb-infected VitD^{HI}, VitD^{LO} and VitD^{Std} mice were collected, stimulated *ex vivo* and used for flow cytometric analysis of CD4, CD8, IFNγ, and TNFα. (**A–C**) Representative dot plots showing CD4 and CD8 staining of cells from VitD^{LO} and VitD^{HI} MLNs on (**A**) day 25, (**B**) day 35 and (**C**) day 92 post-infection; the numbers on each dot plot indicate the frequency of cells that were positive for each marker. (**D–G**) Frequency values from 3–4 mice per group per timepoint were combined to show changes in (**D**) CD4$^+$, (**E**) CD8$^+$, (**F**) CD4$^+$IFNγ$^+$, (**G**) CD4$^+$TNFα$^+$, (**H**) CD8$^+$IFNγ$^+$ and (**I**) CD8$^+$TNFα$^+$ frequency over time. The data points in (**D–I**) represent the mean frequency (± SD) of positive cells at each time point (open circles, VitD^{LO}; closed squares, VitD^{HI}). The brown shaded area in each graph represents the standard deviation of each population frequency in Mtb-infected VitD^{Std} mice over the same timecourse. *, $p \leq 0.05$, Student's *t* test).

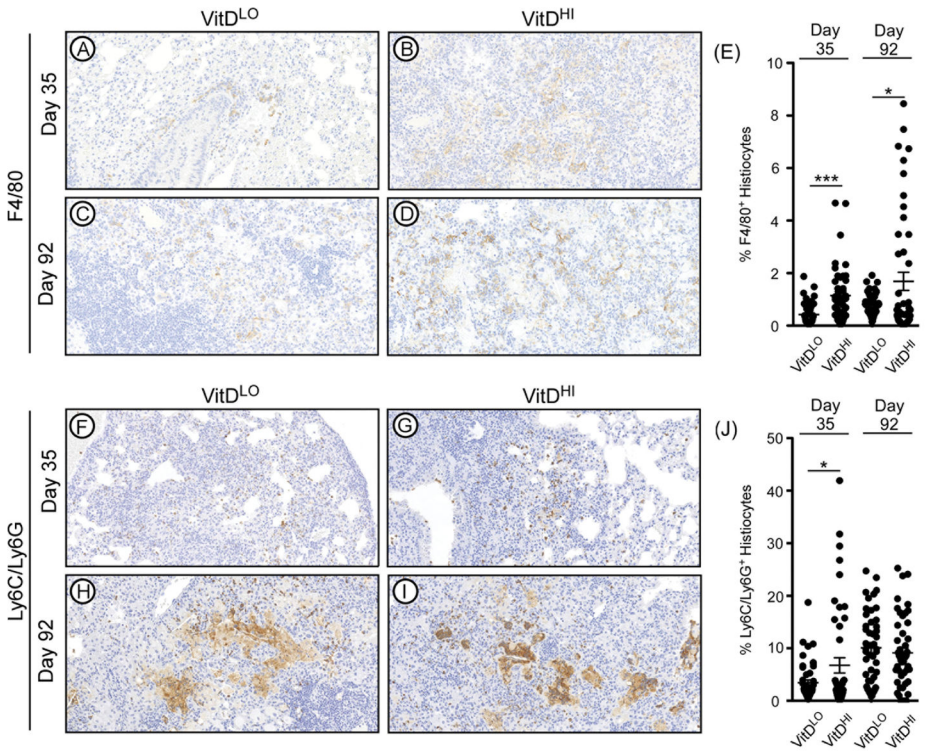

FIGURE 5. Dietary VitD$_3$ alters the representation of F4/80$^+$ and Ly6C/Ly6G$^+$ lineages in Mtb-infected lungs

Immunohistochemistry using antibodies specific to (**A–D**) F4/80 and (**F–I**) Ly6C/Ly6G was used to determine the frequency of histiocytes expressing each respective marker in the granulomatous regions of (**A, C, F, H**) VitD^{LO} mice and (**B, D, G, I**) VitD^{HI} mice on (**A–B, F–G**) post-infection day 35 and (**C–D, H–I**) post-infection day 92. Shown in (**A–D, F–I**) are representative images of each stain along with (**E, J**) the results of our using digital immunochemistry analysis to determine the (**E**) frequency of histiocytes that are F4/80$^+$ and (**J**) frequency of histiocytes that are Ly6C/Ly6G$^+$. Each data point in (**E, J**) represents the frequency of positive cells in one granulomatous region of one mouse; ~50 ROI per group (4 mice/group) were analyzed in this manner. ***, $p \leq 0.0005$ as determined by Student's t-test; *, $p \leq 0.05$ as determined by Student's t-test.

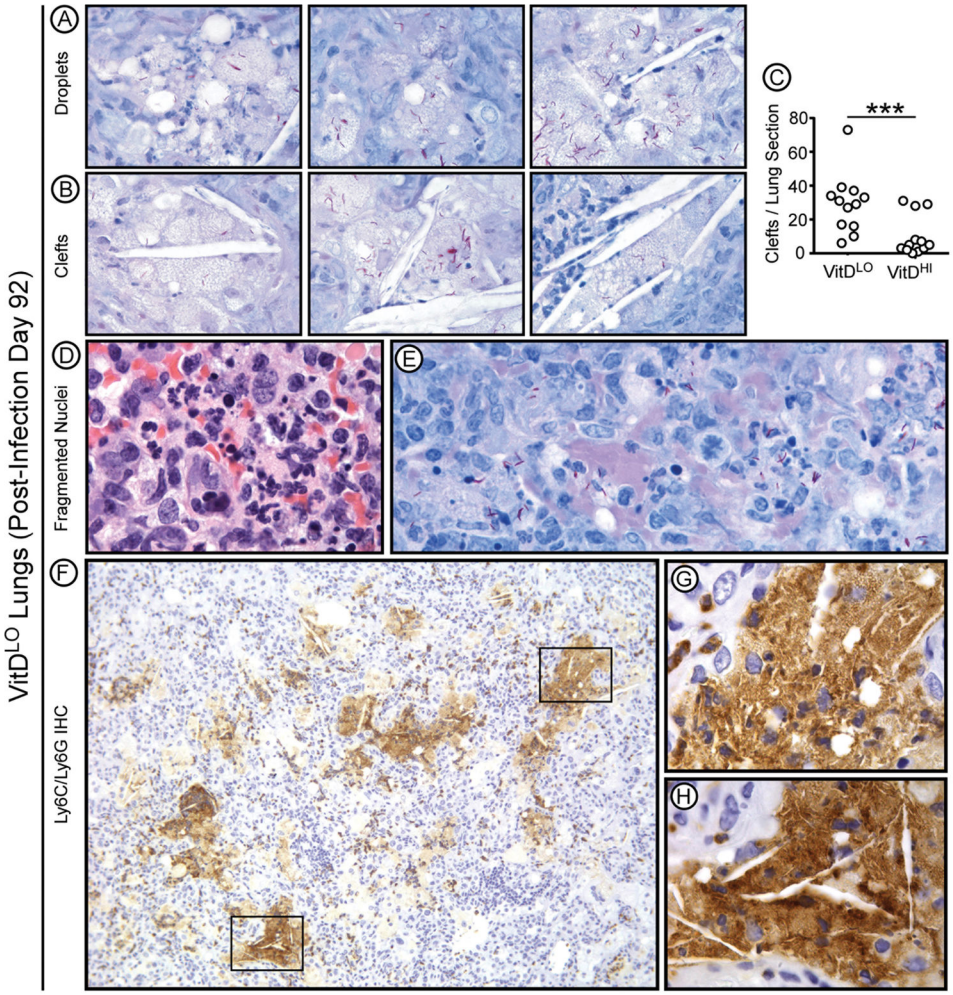

FIGURE 6. Dietary $VitD_3$ suppresses pulmonary immunopathology during late stage TB

(**A–B**) Shown are representative images demonstrating AFB localization in or near (**A**) lipid droplets and (**B**) cholesterol clefts in the lungs of $VitD^{LO}$ mice, the group in which cholesterol clefts were the most prominent. (**C**) Quantitative analysis of cholesterol cleft abundance in $VitD^{LO}$ and $VitD^{HI}$ lungs. (**D–E**) On post-infection day 92, AFB in $VitD^{LO}$ mice were also found in proximity to areas containing fragmented nuclei. Shown in (**D**) is an H&E stain of one such area, which we used to confirm that puncta represented fragmented nuclei (i.e. stained with hematoxylin). Shown in (**E**) is a representative lung section demonstrating the presence of AFB near fragmented nuclei. (**F–H**) Mtb-infected $VitD^{LO}$ lungs were examined for the localization of $Ly6C/Ly6G^+$ cells along cholesterol clefts. Shown is (**F**) a representative 10× micrograph containing several distinct cleft-containing areas that are surrounded by $Ly6C/Ly6G^+$ tissue. (**G–H**) Two of the cleft-containing areas in (**F**) are demarcated and shown at 100× magnification. ***, $p \leq 0.0005$ as determined by Student's t-test.

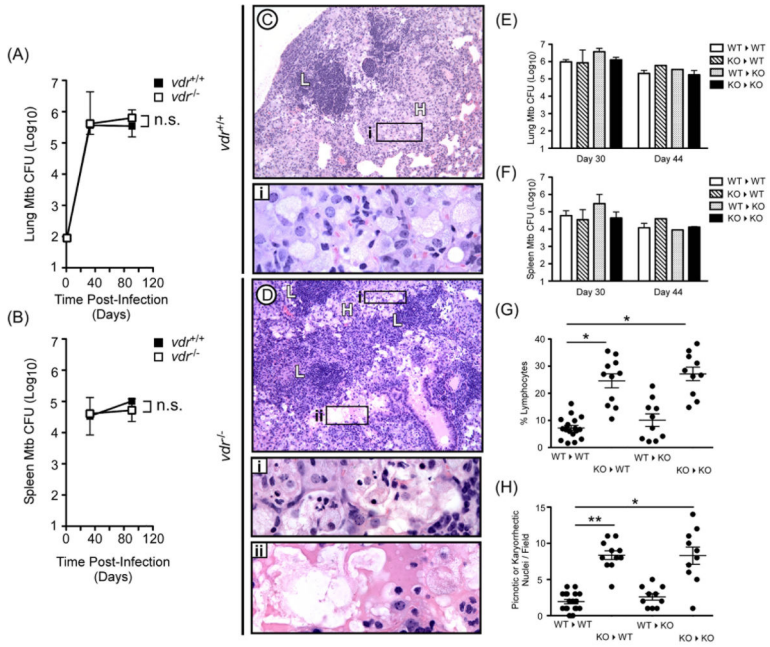

FIGURE 7. Hematopoietic VitD-responsiveness is required to limit TB immunopathology

(**A–D**) Groups of *vdr*$^{+/+}$ and *vdr*$^{-/-}$ mice were simultaneously infected via aerosol with Mtb H37Rv. At select times post-infection, Mtb burdens in the lungs (**A**) and spleen (**B**) were determined. Shown for each time is the mean number of CFU (log10) present in 3–4 mice per genotype per time point. (**C–D**) At post-infection day 90, lung sections from *vdr*$^{+/+}$ and *vdr*$^{-/-}$ mice were stained with H&E to visually assess the degree of pulmonary pathology. Shown is (**C**) a 10× magnification of a representative *vdr*$^{+/+}$ granulomatous region showing the presence of both lymphocyte- and histiocyte-rich areas (marked by an "L" and "H", respectively); shown below in inset **Ci** is a 100× magnification of the histiocyte-rich area, in which cells and nuclei are largely intact. Similarly depicted is (**D**) a 10× magnification of a representative *vdr*$^{-/-}$ granulomatous region containing both lymphocyte (L)- and histiocyte (H)-rich areas; in contrast to *vdr*$^{+/+}$ mice, and shown at 100× magnification in the insets below, the histiocyte-rich areas of *vdr*$^{-/-}$ granulomatous regions contain (inset **Di)** numerous picnotic or karyorrhectic nuclei and (inset **Dii**) evidence of parenchyma destruction. (**E–H**) Four groups of radiation bone marrow chimeras (*vdr*$^{+/+}$ → *vdr*$^{+/+}$, *vdr*$^{-/-}$ → *vdr*$^{+/+}$, *vdr*$^{+/+}$ → *vdr*$^{-/-}$, and *vdr*$^{-/-}$ → *vdr*$^{-/-}$ mice) were simultaneously infected; on post-infection days 30 and 44, Mtb burden in the (**E**) lungs and (**F**) spleen of each group was determined. Shown for each organ is the mean (±SD) number of CFU present at these times. (**G–H**) H&E stained lung sections from chimeric mice were used to identify the granulomatous region present at post-infection day 44; morphometric analysis was then used to quantify (**G**) the extent to which lymphocytes contributed to the area of each granulomatous region, and (**H**) the total number of picnotic or karyorrhectic nuclei per visual field. *, $p \leq 0.05$ and **, $p \leq 0.005$ as determined by ANOVA; n.d., not significantly different.